

Stellar Obliquities in Long-period Exoplanet Systems (SOLES) I: The Spin-Orbit Alignment of K2-140 b

MALENA RICE,^{1,*} SONGHU WANG,² ANDREW W. HOWARD,³ HOWARD ISAACSON,^{4,5} FEI DAI,⁶ XIAN-YU WANG,^{7,8} COREY BEARD,⁹ AIDA BEHMARD,^{6,*} CASEY BRINKMAN,^{10,*} RYAN A. RUBENZAHL,^{3,*} AND GREGORY LAUGHLIN¹

¹*Department of Astronomy, Yale University, New Haven, CT 06511, USA*

²*Department of Astronomy, Indiana University, Bloomington, IN 47405, USA*

³*Department of Astronomy, California Institute of Technology, Pasadena, CA 91125, USA*

⁴*Department of Astronomy, University of California Berkeley, Berkeley CA 94720, USA*

⁵*Centre for Astrophysics, University of Southern Queensland, Toowoomba, QLD, Australia*

⁶*Division of Geological and Planetary Sciences, California Institute of Technology, Pasadena, CA 91125, USA*

⁷*National Astronomical Observatories, Chinese Academy of Sciences, Beijing 100012, China*

⁸*University of the Chinese Academy of Sciences, Beijing, 100049, China*

⁹*Department of Physics and Astronomy, University of California Irvine, Irvine, CA 92697, USA*

¹⁰*Institute for Astronomy, University of Hawai'i at Manoa, Honolulu, HI 96822, USA*

ABSTRACT

Obliquity measurements for stars hosting relatively long-period giant planets with weak star-planet tidal interactions may play a key role in distinguishing between formation theories for shorter-period hot Jupiters. Few such obliquity measurements have been made to date due to the relatively small sample of known wide-orbiting, transiting Jovian-mass planets and the challenging nature of these targets, which tend to have long transit durations and orbit faint stars. We report a measurement of the Rossiter-McLaughlin effect across the transit of K2-140 b, a Jupiter-mass planet with period $P = 6.57$ days orbiting a $V = 12.6$ star. We find that K2-140 is an aligned system with projected spin-orbit angle $\lambda = 0.5^\circ \pm 9.7^\circ$, suggesting a dynamically cool formation history. This observation builds towards a population of tidally detached giant planet spin-orbit angles that will enable a direct comparison with the distribution of close-orbiting hot Jupiter orbital configurations, elucidating the prevalent formation mechanisms of each group.

Keywords: planetary alignment (1243), exoplanet dynamics (490), star-planet interactions (2177), exoplanets (498), planetary theory (1258), exoplanet systems (484)

1. INTRODUCTION

The obliquity of a star, or the degree of alignment between the star's spin axis and its companion planets' net orbital angular momentum axis, provides crucial insights into the dynamical evolution of the surrounding system. Trends in stellar obliquity can constrain the prevalence of various processes crafting the observed distribution of extrasolar planets (e.g. Winn et al. 2010; Albrecht et al. 2012; Winn & Fabrycky 2015).

While the obliquities of many hot-Jupiter-hosting stars have been determined through measurements of the Rossiter-McLaughlin effect (Rossiter 1924; McLaughlin 1924), only a handful of these measurements have been made for systems with planets orbiting at larger distances from their host star, where star-planet tidal interactions are too weak to significantly influence the planets' orbital alignment. We refer to these wide-orbiting planets as “tidally detached.” Because the probability p of transit for a given planet with semimajor axis a falls as $p \propto 1/a$, fewer tidally detached transiting giant planets have been discovered to date as compared with closer-in hot Jupiters. Due to the volume-limited sample of bright stars, those tidally detached Jupiters that have been discovered are often challenging Rossiter-McLaughlin targets, orbiting stars too faint to obtain a

Corresponding author: Malena Rice
malena.rice@yale.edu

* NSF Graduate Research Fellow

sufficient number of high-resolution spectroscopic observations across a single transit with any but the largest existing ground-based telescopes.

The vast majority of spin-orbit angle measurements have, consequently, been made for planets on tight orbits with $a/R_* \lesssim 12$. However, the obliquities of stars hosting wider-separation giant planets may provide the evidence necessary to distinguish between the various proposed formation mechanisms for hot Jupiters (Winn & Fabrycky 2015; Dawson & Johnson 2018). Furthermore, in the classical quiescent formation framework for hot and warm Jupiters, the long tidal realignment timescales of these systems enable a direct measurement of the primordial dispersion in protoplanetary disk misalignments.

We present a Rossiter-McLaughlin measurement across the transit of K2-140 b with the High Resolution Echelle Spectrometer (HIRES; Vogt et al. 1994) on the 10-meter Keck I telescope. K2-140 (EPIC 228735255) is a $V = 12.6$ G5 star hosting a $1.019 \pm 0.070 M_J$ planet, K2-140 b, with a $P = 6.57$ -day orbital period (Giles et al. 2018). With $a/R_* = 12.88$, K2-140 b is one of the widest-separation tidally detached planets to date with a measured spin-orbit angle. This is the first measurement in our Stellar Obliquities in Long-period Exoplanet Systems (SOLES) survey designed to expand the sample of Rossiter-McLaughlin measurements for wide-separation exoplanets.

K2-140 b was first characterized using photometry from the *K2* mission (Howell et al. 2014), a re-purposed extension of the *Kepler* mission (Borucki et al. 2010), after two of its reaction wheels failed. Giles et al. (2018) used radial velocity (RV) observations from CORALIE (Queloz et al. 2000) and the High Accuracy Radial velocity Planet Searcher (HARPS; Pepe et al. 2000) to confirm the planetary nature of K2-140 b and to constrain its physical and orbital properties.

The planet was independently characterized in Korth et al. (2019), which incorporated RV data from the Fibre-fed Échelle Spectrograph (FIES) (Telting et al. 2014) within their analysis. While Giles et al. (2018) found a low but nonzero eccentricity for the planet ($e = 0.120^{+0.056}_{-0.046}$), Korth et al. (2019) found that the planet was consistent with $e = 0$. Data from both of these past studies is incorporated within our joint analysis.

2. OBSERVATIONS

We obtained 18 radial velocity measurements of K2-140 with the Keck/HIRES instrument from 9:25-15:40 UT on Feb 24, spanning a full transit of K2-140 b. Conditions were favorable throughout most of the observing

period, with typical seeing ranging from $1.0'' - 1.3''$. A spike in humidity during the post-transit baseline observations led to a telescope dome closure at 14:40 UT, resulting in a ~ 40 -minute gap in data before the last radial velocity measurement.

All RV observations were obtained using the C2 decker ($14'' \times 0.861''$, $R = 60,000$) and an iodine absorption cell, which imprints a dense forest of molecular iodine features onto each spectrum to enable high Doppler precision (Butler et al. 1996). The $14''$ length of the C2 decker allows for direct sky subtraction, improving RV precision for faint stars such as K2-140. The median exposure time was 1,119 seconds, with $\sim 34k$ exposure meter counts per spectrum.

Our dataset was reduced using the California Planet Search pipeline outlined in Howard et al. (2010), and we obtained a typical signal-to-noise ratio of 71 per pixel from the reduced spectra. The HIRES radial velocity results and uncertainties can be found in Table 1 and are shown in the rightmost panel of Figure 1. We include the S-index and associated uncertainty at each observation in Table 1 for reference.

We also obtained a 45-minute iodine-free HIRES exposure of K2-140 using the B3 decker ($14.0'' \times 0.574''$, $R = 72,000$) two nights after the measurement of the Rossiter-McLaughlin effect, during UT Feb 26. This template observation was used to calibrate our RVs and to precisely determine stellar parameters (see Section 4). Conditions were favorable during this measurement, and seeing was $1.2''$. Our reduced template had a signal-to-noise ratio of 123 per pixel (106k exposure meter counts).

3. OBLIQUITY MODELING

To determine the sky-projected spin-orbit angle λ for K2-140 b, we used the `allesfitter` Python package (Günther & Daylan 2020) to jointly model the in-transit HIRES radial velocity data together with photometry from *K2* and archival radial velocity datasets available from the FIES, CORALIE, and HARPS spectrographs.

All fitted parameters listed in Table 2 were allowed to vary, and each parameter was initialized with uniform priors. Initial guesses for P , T_0 , $\cos i$, R_p/R_* , $(R_* + R_p)/a$, K , $\sqrt{e} \cos \omega$, and $\sqrt{e} \sin \omega$ were obtained using values from Giles et al. (2018). The two limb darkening coefficients q_1 and q_2 were each initialized with values of 0.5. We accounted for potential radial velocity offsets between each separate spectrograph, with priors bounded by ± 1000 m/s. Jitter terms were modeled separately for each instrument and added in quadrature to

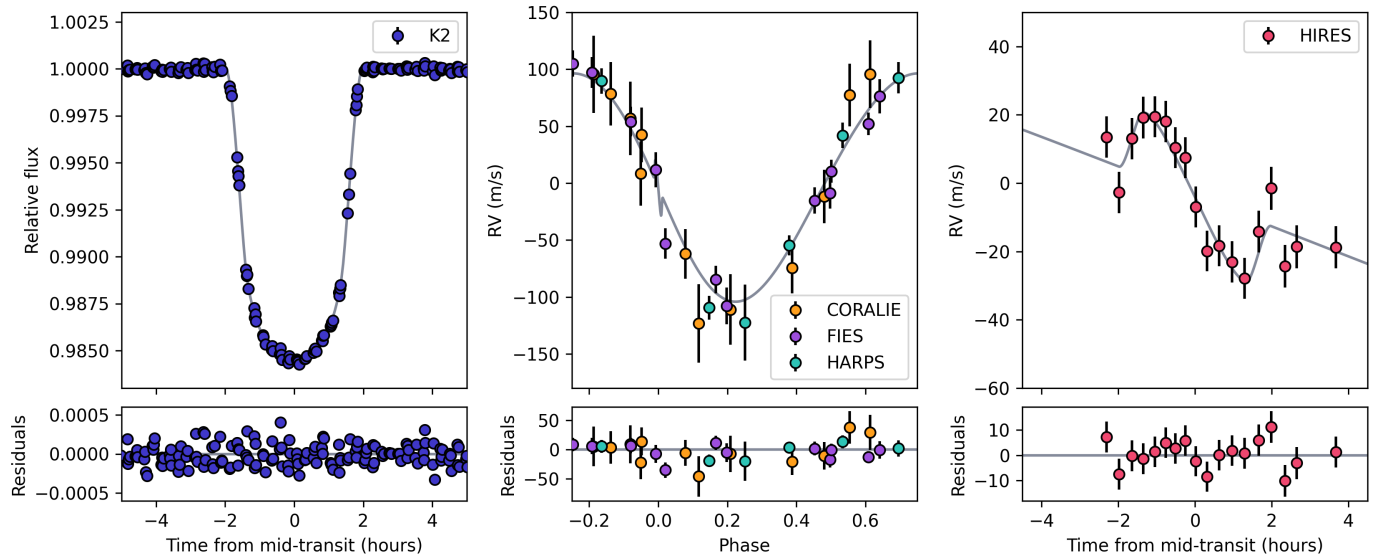


Figure 1. Joint fit to photometry, out-of-transit RV data, and the in-transit Rossiter-McLaughlin RV data obtained for K2-140 b. The model is shown in gray, while data is provided in color with modeled constant offsets and jitter terms included. The associated residuals are provided below each panel.

Table 1. HIRES radial velocities for the K2-140 system.

Time (BJD)	RV (m/s)	σ_{RV} (m/s)	S-index	σ_S
2459269.903807	17.62	2.48	0.165	0.001
2459269.917697	1.43	2.59	0.166	0.001
2459269.931633	17.18	2.55	0.160	0.001
2459269.944029	23.36	2.58	0.168	0.001
2459269.956264	23.63	2.38	0.161	0.001
2459269.968059	22.22	2.47	0.166	0.001
2459269.978707	14.54	2.35	0.159	0.001
2459269.989634	11.66	2.34	0.160	0.001
2459270.000977	-2.85	2.31	0.165	0.001
2459270.013142	-15.76	2.19	0.167	0.001
2459270.026233	-14.19	2.41	0.163	0.001
2459270.040065	-18.89	2.45	0.160	0.001
2459270.054024	-23.71	2.41	0.159	0.001
2459270.069384	-10.01	2.63	0.161	0.001
2459270.083054	2.645	2.96	0.155	0.001
2459270.097753	-20.13	2.85	0.152	0.001
2459270.110694	-14.47	3.08	0.147	0.001
2459270.153058	-14.61	2.71	0.155	0.001

the instrumental uncertainties. λ was allowed to vary between -180° and $+180^\circ$.

We ran an affine-invariant Markov Chain Monte Carlo (MCMC) analysis with 100 walkers to sample the posterior distributions of all model parameters. The best-fit model parameters and their associated 1σ uncertainties were extracted after obtaining 500,000 accepted steps per walker. Our results are listed in Table 2 and are in good agreement with the associated values obtained by Giles et al. (2018) and Korth et al. (2019).

The best-fit joint model is shown in Figure 1 together with each dataset included in the analysis, as well as the residuals of each fit. The fitted and derived parameters corresponding to this model are provided in Table 2. We obtain a low but nonzero eccentricity $e = 0.069^{+0.042}_{-0.028}$ for K2-140 b, in agreement with the value derived by Giles et al. (2018). K2-140 is consistent with alignment, with $\lambda = 0.5^\circ \pm 9.7^\circ$ and $v \sin i_* = 2.51 \pm 0.38$ km/s.

4. STELLAR PARAMETERS

An understanding of host star properties can help to contextualize the evolutionary pathways through which a system may have reached its current state. We extracted stellar parameters from our Keck/HIRES template spectrum of K2-140 using the data-driven spectroscopic modeling program *The Cannon* (Ness et al. 2015; Casey et al. 2016), following the methods of Rice & Brewer (2020).

Given a set of uniformly processed input training spectra and associated stellar “labels” – that is, stellar parameters and elemental abundances – *The Cannon* constructs a generative model describing the probability density function of flux at each wavelength as a function of the labels. The model can then be applied to a new set of spectra, uniformly processed in the same manner as the training set, to obtain the associated stellar labels.

We trained *The Cannon* using the uniformly analyzed Spectral Properties of Cool Stars (SPOCS) catalogue (Brewer et al. 2016) of 18 stellar labels, including 3

Table 2. System properties derived for K2-140.

Parameter	Description	Priors	Value	+1 σ	-1 σ
Fitted Parameters:					
R_p/R_*	Planet-to-star radius ratio	$\mathcal{U}(0; 1)^*$	0.1163	0.0012	0.0011
$(R_* + R_p)/a$	Sum of radii divided by the orbital semimajor axis	$\mathcal{U}(0; 1)$	0.0960	0.0043	0.0039
$\cos i$	Cosine of the orbital inclination	$\mathcal{U}(0; 1)$	0.0518	0.0053	0.0048
T_0	Mid-transit epoch (BJD)	2458435.7138 [†]	2458429.1426	0.0015	0.0015
P	Orbital period (days)	$\mathcal{U}(5.569188; 7.569188)$	6.569199	1.2e-05	1.2e-05
K	Radial velocity semi-amplitude (m/s)	$\mathcal{U}(0; 1000)$	106.5	4.7	4.7
$\sqrt{e} \cos \omega$	Eccentricity parameter 1	$\mathcal{U}(-1.0; 1.0)$	-0.156	0.067	0.053
$\sqrt{e} \sin \omega$	Eccentricity parameter 2	$\mathcal{U}(-1.0; 1.0)$	0.189	0.098	0.15
q_1	Quadratic limb darkening coefficient 1	$\mathcal{U}(0.0; 1.0)$	0.74	0.15	0.14
q_2	Quadratic limb darkening coefficient 2	$\mathcal{U}(0.0; 1.0)$	0.175	0.072	0.055
$\Delta_{RV, FIES}$	RV offset, FIES (m/s)	$\mathcal{U}(-1000.0; 1000.0)$	1.1287	0.0044	0.0042
$\Delta_{RV, CORALIE}$	RV offset, CORALIE (m/s)	$\mathcal{U}(-1000.0; 1000.0)$	1.2141	0.0083	0.0083
$\Delta_{RV, HARPS}$	RV offset, HARPS (m/s)	$\mathcal{U}(-1000.0; 1000.0)$	1.2459	0.0053	0.0053
$\Delta_{RV, HIRES}$	RV offset, HIRES (m/s)	$\mathcal{U}(-1000.0; 1000.0)$	0.0051	0.0034	0.0034
λ	Sky-projected spin-orbit angle ($^\circ$)	$\mathcal{U}(-180.0; 180.0)$	0.5	9.7	9.7
$v \sin i_*$	Sky-projected stellar rotational velocity (km/s)	$\mathcal{U}(0.0; 20.0)$	2.51	0.38	0.38
Derived Parameters:					
R_p	Planetary radius (R_J)	...	1.203	0.076	0.076
M_p	Planetary mass (M_J)	...	1.13	0.12	0.11
b	Impact parameter	...	0.574	0.022	0.022
T_{14}	Transit duration (h)	...	3.946	0.016	0.016
δ	Transit depth	...	0.015490	4.2e-05	4.2e-05
a	Semimajor axis (au)	...	0.0575	0.0046	0.0043
i	Inclination ($^\circ$)	...	87.03	0.27	0.30
e	Eccentricity	...	0.069	0.042	0.028
ω	Argument of periastron ($^\circ$)	...	131	38	20
u_1	Limb darkening parameter 1	...	0.300	0.088	0.080
u_2	Limb darkening parameter 2	...	0.56	0.15	0.16

* $\mathcal{U}(a; b)$ is a uniform prior with lower and upper limits a and b , respectively.

[†] We provided a reference value for T_0 . During the fit, `allesfitter` can shift epochs to the data center to derive an optimal T_0 .

global stellar parameters (T_{eff} , $\log g$, $v \sin i_*$), and 15 elemental abundances: C, N, O, Na, Mg, Al, Si, Ca, Ti, V, Cr, Mn, Fe, Ni, and Y. The sample of 1202 Keck/HIRES spectra vetted in Rice & Brewer (2020) was applied as our training/test set.

The continuum baseline of each spectrum was uniformly fit and divided out using the iterative polynomial fitting procedure outlined in Valenti & Fischer (2005). Then, we split the SPOCS sample into an 80%/20% training/test split, applied the telluric mask from Rice & Brewer (2020) to all spectra, and trained the model, using the scatter of the test set results to determine the uncertainties of each extracted parameter. Finally, the trained model was applied to the newly acquired K2-140 Keck/HIRES template spectrum. A segment of the obtained model spectrum is shown in comparison with the HIRES template data in Figure 2.

Our results are provided in Table 3 together with estimates from previous works for reference. Our values

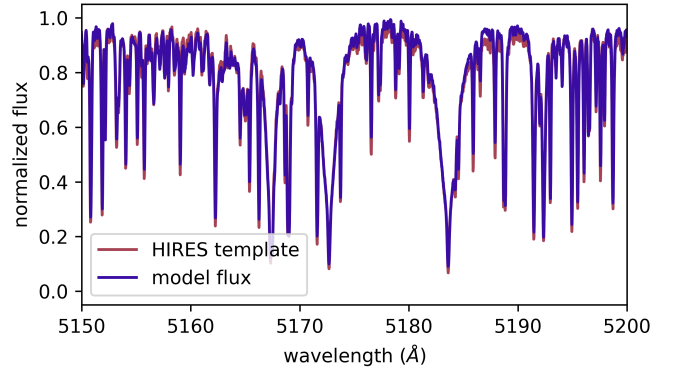


Figure 2. Sample segment of the model spectrum returned by *The Cannon*, shown alongside the K2-140 HIRES template spectrum in the vicinity of the Mg Ib triplet (lines at 5167, 5172, and 5183 Å).

for T_{eff} , $\log g$, and $[\text{Fe}/\text{H}]$ are in agreement with those acquired in previous studies. The $v \sin i_*$ value obtained using *The Cannon* is lower than previous estimates but

is in agreement with the RM joint fit results and [Korth et al. \(2019\)](#) within 1σ . We find that K2-140 is metal-enriched relative to solar abundances, consistent with past evidence showing that short-period giant planets are more common around metal-rich stars ([Fischer & Valenti 2005](#)).

5. DISCUSSION

5.1. Implications of the Low λ of K2-140 b

At $T_{\text{eff}} = 5585$ K, K2-140 should have a convective envelope. In the framework of equilibrium tides, the planet’s timescale for realignment from turbulent friction would thus follow

$$\tau_{CE} = \frac{10^{10}\text{yr}}{(M_p/M_*)^2} \left(\frac{a/R_*}{40}\right)^6, \quad (1)$$

where τ_{CE} is the realignment timescale for host stars with convective envelopes, and M_p/M_* is the planet-to-star mass ratio ([Zahn 1977](#); [Albrecht et al. 2012](#)). For K2-140 b, $\tau_{CE} = 1.2 \times 10^{13}$ yr, longer than the age of the Universe. As a result, we conclude that K2-140 b was likely aligned at the time of protoplanetary disk dispersal.

The theory of equilibrium tides presented in Equation 1 is employed as a simplified heuristic for a broader theoretical framework that has substantially advanced over recent years ([Ogilvie 2014](#)). A key problem in the equilibrium tides framework is that, under standard assumptions, hot Jupiters should experience rapid orbital decay. [Lai \(2012\)](#) demonstrated that one component of the tidal potential (the “obliquity tide”) can excite inertial waves in the convective envelopes of cool stars, which, when damped, can enhance dissipation of the stellar obliquity without shrinking the companion’s orbit. Obliquity tides have been further explored in additional work ([Ogilvie 2013](#); [Lin & Ogilvie 2017](#); [Anderson et al. 2021](#)). While obliquity tides are not included in our analysis, previous work has demonstrated that Equation 1 is a useful heuristic revealing that low-obliquity systems tend to have shorter tidal timescales than high-obliquity systems ([Albrecht et al. 2012](#)).

K2-140 b is one of only 13 giant planets with a measured spin-orbit angle at $a/R_* > 12$, as shown in the left panel of Figure 3. Of these planets, it is one of only a few with an aligned orbit despite its long tidal realignment timescale. The alignment of K2-140 b suggests that at least some hot Jupiters form through quiescent pathways, such as in-situ formation or disk migration in an initially aligned disk.

The highly misaligned planets at large a/R_* each have high eccentricities (right panel of Figure 3), indicative of

strong dynamical interactions that may have produced both elevated obliquities and eccentricities. The coexistence of this population with the dynamically quiescent K2-140 system at large a/R_* suggests that there are multiple hot Jupiter formation channels.

No neighboring planets have yet been found in the K2-140 system, despite previous observations showing that inner, coplanar companions are common for slightly longer-period warm Jupiters ($10 < P < 200$ days; [Huang et al. 2016](#)) and predictions that outer, mutually-inclined companions with $P \lesssim 100$ days should be regularly produced by in-situ hot Jupiter formation via core accretion ([Batygin et al. 2016](#)). However, additional low-mass or distant planets in the system cannot be ruled out by the existing observations, with radial velocity residuals of tens of m/s and an observing baseline of only ~ 4 years.

5.2. Motivation for Additional Obliquity Measurements in Tidally Detached Systems through SOLES

Existing Rossiter-McLaughlin measurements of wide-orbiting planets suggest that this population may have an intrinsically different spin-orbit angle distribution from the shorter-period hot Jupiter population. In particular, the trend of systematically lower obliquities observed for stars at temperatures below the Kraft break ($T_{\text{eff}} \approx 6100$ K; [Kraft 1967](#); [Winn et al. 2010](#); [Schlaufman 2010](#)), which may result from tidal damping (e.g. [Wang et al. 2021](#)), is not immediately evident at longer orbital periods, as shown in Figure 4.

Conversely, Figure 4 reveals tentative (2.79σ) evidence that relatively long-period planets ($P > 5$ days) around hot stars are preferentially *less* misaligned than their shorter-period counterparts. Furthermore, the most misaligned $P > 5$ day planet in the middle panel, KELT-6 b ($P = 7.8$ days, $|\lambda| = 36 \pm 11^\circ$; [Damasso et al. 2015](#)), orbits a star directly bordering the nominal Kraft break ($T_{\text{eff}} = 6102$ K; [Collins et al. 2014](#)), making it an ambiguous member of its group. We note that hot stars typically have larger radii and thus stronger tidal dissipation at a given orbital period; however, a similar trend has also been previously suggested for a smaller population of planets at large a/R_* ([Yu et al. 2018](#)).

Longer-period planets have comparatively long tidal alignment timescales, especially around hot stars. The small spin-orbit angles observed for exoplanets around hot stars, therefore, may suggest that protoplanetary disks tend to be aligned at the time of gas dispersal (in contrast with a primordial spin-orbit misalignment from a tilted disk; [Batygin 2012](#); [Spalding & Batygin 2015](#)). In this case, hot Jupiters would need to obtain their misalignments after the protoplanetary disk has dispersed,

Table 3. Stellar parameters for K2-140.

Parameter	Unit	The Cannon (this work)	RM joint fit (this work)	Giles+ 2019	Korth+ 2019
T_{eff}	K	5610 ± 59	-	5654 ± 55	5585 ± 120
$\log g$	cm/s^2	4.4 ± 0.1	-	$4.452^{+0.010}_{-0.009}$	4.4 ± 0.2
$v \sin i_*$	km/s	2.31 ± 1.07	2.51 ± 0.38	3.8 ± 0.2	3.6 ± 1.0
[Fe/H]	dex	0.18 ± 0.04	-	0.12 ± 0.045	0.10 ± 0.10
[C/H]	dex	0.14 ± 0.08	-	-	-
[N/H]	dex	0.05 ± 0.09	-	-	-
[O/H]	dex	0.06 ± 0.09	-	-	-
[Na/H]	dex	0.13 ± 0.07	-	-	0.12 ± 0.10
[Mg/H]	dex	0.12 ± 0.04	-	-	0.27 ± 0.10
[Al/H]	dex	0.22 ± 0.13	-	-	-
[Si/H]	dex	0.18 ± 0.05	-	-	-
[Ca/H]	dex	0.24 ± 0.04	-	-	0.12 ± 0.10
[Ti/H]	dex	0.24 ± 0.05	-	-	-
[V/H]	dex	0.17 ± 0.06	-	-	-
[Cr/H]	dex	0.19 ± 0.05	-	-	-
[Mn/H]	dex	0.18 ± 0.06	-	-	-
[Ni/H]	dex	0.18 ± 0.05	-	-	0.20 ± 0.10
[Y/H]	dex	0.23 ± 0.12	-	-	-

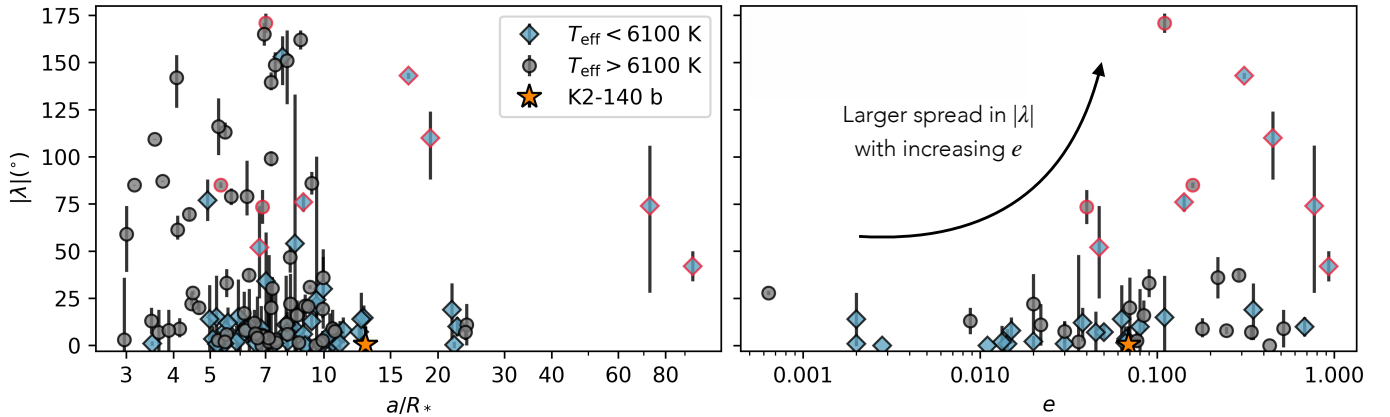


Figure 3. *Left:* K2-140 b relative to other Rossiter-McLaughlin measurements of giant planets ($M > 0.3M_J$) in the TEPCat catalogue (Southworth 2011), with a and R_* obtained through cross-matching with the NASA Exoplanet Archive and missing values filled in from the Extrasolar Planets Encyclopaedia. In a/R_* space, K2-140 b lies just exterior to most planets with measured spin-orbit angles. This makes it one of only a handful of planets with a tidal realignment timescale $\tau \gg$ stellar age, such that it would not have had time to realign if it had been misaligned at the time of protoplanetary disk dispersal. *Right:* Distribution of measured obliquities as a function of eccentricity for planets with $e > 0$. The range of measured λ values is larger at high e for planets orbiting stars both above and below the Kraft break. Planets with $|\lambda| > 40^\circ$ and $e > 0.01$ are outlined in red in both panels. Among the planets with $e \neq 0$, the spread in misalignments is larger at higher eccentricities.

favoring high-eccentricity migration as an important formation mechanism (e.g. Wu & Murray 2003; Fabrycky & Tremaine 2007). Most of the misaligned planets at $P > 5$ days are on eccentric orbits, suggesting that interactions with stellar or planetary companions in the systems may have induced both elevated obliquities and eccentricities.

If a growing sample of spin-orbit angles at $P > 5$ days reveals that cool stars below the Kraft break are preferentially more misaligned than hotter stars above

the Kraft break, this may also be suggestive of interactions with additional companions. In the presence of an external, inclined Jovian-mass companion, spin-orbit misalignments can be excited preferentially in cool star systems due to a secular resonance between the host star’s spin axis precession frequency and nodal precession induced by interactions with the companion (Anderson & Lai 2018). Cool stars spin down over time due to magnetic braking, enabling this resonant excitation. Hot stars, by contrast, lack a convective envelope and

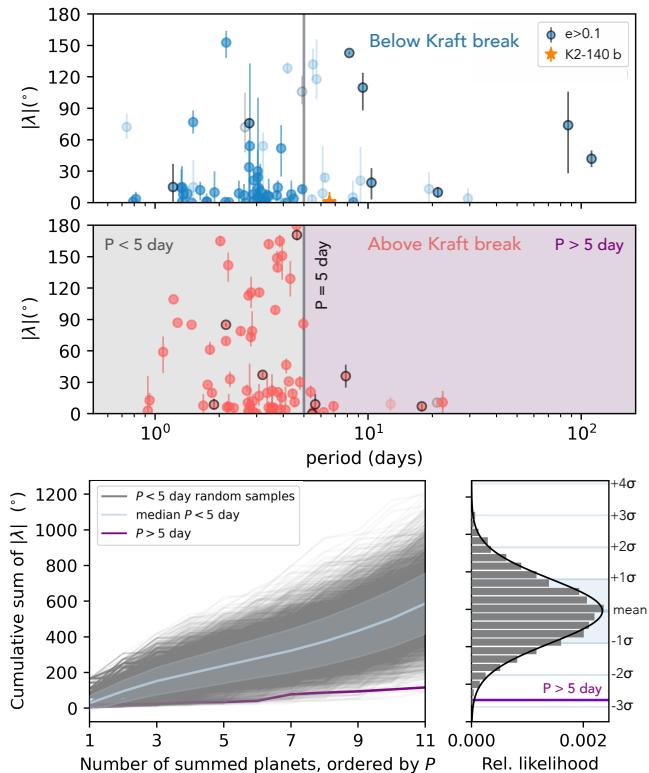


Figure 4. Obliquity distribution of all stars below (top panel) and above (middle panel) the Kraft break with measured λ values in the TEPICat catalogue, provided as a function of the companion planet’s orbital period. Measurements for companion planets with $e > 0.1$ are bordered in black. Measurements for companion planets with $M < 0.3M_J$ are shown at lower opacity. The cumulative sums in the bottom panel include only planets above the Kraft break, comparing the $P > 5$ day population (purple) with 5000 $P < 5$ day samples (gray), randomly sampled without replacement. The histogram on the bottom right shows a vertical cut through the final cumulative sum distribution. The $P > 5$ day cumulative sum is a 2.79σ outlier from the random draw distribution.

continue to rapidly rotate over their lifetimes. As a result, irrespective of the external giant planet companion rate around hot stars, this mechanism should occur only in cool star systems.

The substantially inclined companions necessary to induce this mechanism would also be capable of exciting the inner planet’s orbital eccentricity. This may be reflected by the apparent increase in both misalignments and eccentricities for long-period planets around cool stars, shown in the top panel of Figure 4. Conversely, the alignment of K2-140 b and similar planets on low-eccentricity orbits indicates that they should not have

nearby giant planet companions with large ($> 10^\circ$) mutual inclinations within ~ 2 au.

If the trend of large misalignments for cool stars hosting tidally detached planets persists, while misalignments remain small for their hot star counterparts, further monitoring would be warranted to constrain the long-period giant planet companion rate for misaligned cool star systems. Additional observations are needed to parse the emerging relationship between stellar temperature, eccentricity, and obliquity for wide-separation planets.

6. ACKNOWLEDGEMENTS

We thank Konstantin Batygin and Kassandra Anderson for helpful discussions that have refined this work. We also thank the anonymous referee for their helpful suggestions that have improved the quality of this manuscript. M.R. is supported by the National Science Foundation Graduate Research Fellowship Program under Grant Number DGE-1752134. The data presented herein were obtained at the W. M. Keck Observatory, which is operated as a scientific partnership among the California Institute of Technology, the University of California and the National Aeronautics and Space Administration. The Observatory was made possible by the generous financial support of the W. M. Keck Foundation. This work is supported by Astronomical Big Data Joint Research Center, co-founded by National Astronomical Observatories, Chinese Academy of Sciences and Alibaba Cloud. This research has made use of the Keck Observatory Archive (KOA), which is operated by the W. M. Keck Observatory and the NASA Exoplanet Science Institute (NExSci), under contract with the National Aeronautics and Space Administration. This research has made use of the NASA Exoplanet Archive, which is operated by the California Institute of Technology, under contract with the National Aeronautics and Space Administration under the Exoplanet Exploration Program.

Software: `numpy` (Oliphant 2006; Walt et al. 2011; Harris et al. 2020), `matplotlib` (Hunter 2007), `pandas` (McKinney et al. 2010), `scipy` (Virtanen et al. 2020), `allesfitter` (Günther & Daylan 2020), `emcee` (Foreman-Mackey et al. 2013)

Facility: Keck: I (HIRES), Exoplanet Archive, Extrasolar Planets Encyclopaedia

REFERENCES

Albrecht, S., Winn, J. N., Johnson, J. A., et al. 2012, *The Astrophysical Journal*, 757, 18

Anderson, K. R., & Lai, D. 2018, *Monthly Notices of the Royal Astronomical Society*, 480, 1402

- Anderson, K. R., Winn, J. N., & Penev, K. 2021, *The Astrophysical Journal*, 914, 56
- Batygin, K. 2012, *Nature*, 491, 418
- Batygin, K., Bodenheimer, P. H., & Laughlin, G. P. 2016, *The Astrophysical Journal*, 829, 114
- Borucki, W. J., Koch, D., Basri, G., et al. 2010, *Science*, 327, 977
- Brewer, J. M., Fischer, D. A., Valenti, J. A., & Piskunov, N. 2016, *The Astrophysical Journal Supplement Series*, 225, 32
- Butler, R. P., Marcy, G. W., Williams, E., et al. 1996, *Publications of the Astronomical Society of the Pacific*, 108, 500
- Casey, A. R., Hogg, D. W., Ness, M., et al. 2016, arXiv preprint arXiv:1603.03040
- Collins, K. A., Eastman, J. D., Beatty, T. G., et al. 2014, *The Astronomical Journal*, 147, 39
- Damasso, M., Esposito, M., Nascimbeni, V., et al. 2015, *Astronomy & Astrophysics*, 581, L6
- Dawson, R. I., & Johnson, J. A. 2018, *Annual Review of Astronomy and Astrophysics*, 56, 175
- Fabrycky, D., & Tremaine, S. 2007, *The Astrophysical Journal*, 669, 1298
- Fischer, D. A., & Valenti, J. 2005, *The Astrophysical Journal*, 622, 1102
- Foreman-Mackey, D., Hogg, D. W., Lang, D., & Goodman, J. 2013, *PASP*, 125, 306
- Giles, H., Bayliss, D., Espinoza, N., et al. 2018, *Monthly Notices of the Royal Astronomical Society*, 475, 1809
- Günther, M. N., & Daylan, T. 2020, arXiv preprint arXiv:2003.14371
- Harris, C. R., Millman, K. J., van der Walt, S. J., et al. 2020, *Nature*, 585, 357
- Howard, A. W., Johnson, J. A., Marcy, G. W., et al. 2010, *The Astrophysical Journal*, 721, 1467
- Howell, S. B., Sobek, C., Haas, M., et al. 2014, *Publications of the Astronomical Society of the Pacific*, 126, 398
- Huang, C., Wu, Y., & Triaud, A. H. 2016, *The Astrophysical Journal*, 825, 98
- Hunter, J. D. 2007, *Computing in science & engineering*, 9, 90
- Korth, J., Csizmadia, S., Gandolfi, D., et al. 2019, *Monthly Notices of the Royal Astronomical Society*, 482, 1807
- Kraft, R. P. 1967, *The Astrophysical Journal*, 150, 551
- Lai, D. 2012, *Monthly Notices of the Royal Astronomical Society*, 423, 486
- Lin, Y., & Ogilvie, G. I. 2017, *Monthly Notices of the Royal Astronomical Society*, 468, 1387
- McKinney, W., et al. 2010, in *Proceedings of the 9th Python in Science Conference*, Vol. 445, Austin, TX, 51–56
- McLaughlin, D. 1924, *The Astrophysical Journal*, 60
- Ness, M., Hogg, D. W., Rix, H.-W., Ho, A. Y., & Zasowski, G. 2015, *The Astrophysical Journal*, 808, 16
- Ogilvie, G. I. 2013, *Monthly Notices of the Royal Astronomical Society*, 429, 613
- . 2014, *Annual Review of Astronomy and Astrophysics*, 52, 171
- Oliphant, T. E. 2006, *A guide to NumPy*, Vol. 1 (Trelgol Publishing USA)
- Pepe, F., Mayor, M., Delabre, B., et al. 2000, in *Optical and IR telescope instrumentation and detectors*, Vol. 4008, International Society for Optics and Photonics, 582–592
- Queloz, D., Mayor, M., Weber, L., et al. 2000, *Astronomy and Astrophysics*, 354, 99
- Rice, M., & Brewer, J. M. 2020, *The Astrophysical Journal*, 898, 119
- Rossiter, R. 1924, *The Astrophysical Journal*, 60
- Schlaufman, K. C. 2010, *The Astrophysical Journal*, 719, 602
- Southworth, J. 2011, *Monthly Notices of the Royal Astronomical Society*, 417, 2166
- Spalding, C., & Batygin, K. 2015, *The Astrophysical Journal*, 811, 82
- Telting, J., Avila, G., Buchhave, L., et al. 2014, *Astronomische Nachrichten*, 335, 41
- Valenti, J. A., & Fischer, D. A. 2005, *The Astrophysical Journal Supplement Series*, 159, 141
- Virtanen, P., Gommers, R., Oliphant, T. E., et al. 2020, *Nature methods*, 17, 261
- Vogt, S. S., Allen, S. L., Bigelow, B. C., et al. 1994, in *Instrumentation in Astronomy VIII*, Vol. 2198, International Society for Optics and Photonics, 362–375
- Walt, S. v. d., Colbert, S. C., & Varoquaux, G. 2011, *Computing in Science & Engineering*, 13, 22
- Wang, S., Winn, J. N., Addison, B. C., et al. 2021, *The Astronomical Journal*, 162, 50
- Winn, J. N., Fabrycky, D., Albrecht, S., & Johnson, J. A. 2010, *The Astrophysical Journal Letters*, 718, L145
- Winn, J. N., & Fabrycky, D. C. 2015, *ARA&A*, 53, 409
- Wu, Y., & Murray, N. 2003, *The Astrophysical Journal*, 589, 605
- Yu, L., Zhou, G., Rodriguez, J. E., et al. 2018, *The Astronomical Journal*, 156, 250
- Zahn, J.-P. 1977, *Astronomy and Astrophysics*, 57, 383